Hydraulics Research
Wallingford

THE NEARSHORE PROFILE MODEL
INCORPORATING WAVE SPECTRA

H N Southgate, MA

Report SR 201
March 1989

ABSTRACT

A computational model for determining wave and current conditions in nearshore regions, known as the Nearshore Profile Model, has been extended to incorporate wave spectra. The theory of spectral wave transformation used by the model is described, and comparisons between the spectral and monochromatic versions of the model are presented. It is concluded that in most cases where input wave spectra are adequately known, they should be used in preference to the equivalent monochromatic wave.

CONTENTS

    TABLES

    1.   Incident Spectra for Laboratory Tests
    2.   Incident Spectra for Field Tests

    FIGURES

    1.   Model geometry of the Nearshore region
    2.   Experimental arrangement used by Visser (from Visser (1984a))
    3.   Laboratory tests - Pierson-Moskowitz spectrum - longshore current
         velocities
    4.   Laboratory tests - Pierson-Moskowitz spectrum - wave set-up
    5.   Laboratory tests - Pierson-Moskowitz spectrum - wave heights (RMS
         values for spectra)
    6.   Laboratory tests - Top-Hat spectrum - longshore current velocites
    7.   Laboratory tests - Top-Hat spectrum - wave set-up
    8.   Laboratory tests - Top-Hat spectrum - wave heights (RMS values for
         spectra)
    9.   Location of profile line for field tests
    10. Field tests - longshore current velocities
    11. Field tests - wave set-up
    12. Field tests - wave heights (RMS values for spectra)

1   INTRODUCTION

In Southgate (1988 and 1989), a 1-D computational
model of nearshore hydrodynamic processes, known as
the Nearshore Profile Model, has been described. This
model is designed to determine wave and longshore
current conditions at grid points along a line
perpendicular to the coastline, under the assumption
of a straight coast and parallel depth contours (the
1-D approximation). A full interaction between waves,
wave-induced currents and tidal currents is
incorporated, and because of its computational speed,
the model can analyse large numbers of input wave and
tidal conditions rendering it suitable for
investigating long-term nearshore and beach
processes.

In the earlier work, the waves were treated as having
a single frequency and direction (except in the
modelling of wave breaking where a Rayleigh
distribution of wave heights is employed). The
present report describes how the model has been
extended to cater for spectral waves with a spread of
energy over a range of frequencies and directions.
Section 2 describes the theoretical method employed
for this spectral wave modelling, and Section 3
contains a comparison of model runs using spectral and
monochromatic wave input in laboratory and field
situations. Conclusions from these model tests are
given in Section 4. The word 'monochromatic' is used
throughout the report to refer to waves with a single
frequency and direction.

2   THEORY

2.1 Introduction

The theory of the spectral wave model is based on
regarding the wave spectrum as composed of a number of
individual frequency and directional components, each
containing a certain amount of wave energy. The

propagation of each component is considered
independently of the others, except in the modelling
of non-linear processes. In the present model the
phenomena of refraction and shoaling (by both depth
variations and currents) are treated linearly, while
energy dissipation by bottom friction and wave
breaking are non-linear processes.

2.2 Wave kinematics

In this section the term 'absolute' refers to wave
quantities measured relative to the seabed, and
'relative' refers to wave quantities measured relative
to an observer moving with the current. The
determination of kinematic quantities requires the
solution to the wave dispersion relation in the
presence of currents,

$$\omega_a - Uk \cos(\delta - \alpha) = (gk \tanh kh)^{\frac{1}{2}} \qquad 2.2.1$$

In this equation ω_a is the absolute angular wave
frequency, U is the current velocity, k is the
wavenumber, δ is the current direction, α is the wave
orthogonal direction, g is the acceleration due to
gravity, and h is the water depth. Figure 1 shows the
definition of angle quantities.

Equation 2.2.1 is solved for the wavenumber, k, in
terms of known values of the other variables at each
grid point and for each spectral component. Once k is
known the following kinematic quantities are
calculated for each spectral component.

a) Relative angular wave frequency,

$$\omega_r = \omega_a - Uk \cos(\delta - \alpha) \qquad 2.2.2$$

b) Relative wave celerity,

$$C_r = \frac{\omega_r}{k} \qquad\qquad 2.2.3$$

c) Relative group velocity,

$$C_{gr} = \frac{C_r}{2} \left[1 + \frac{2kh}{\text{Sinh } (2kh)}\right] \qquad\qquad 2.2.4$$

d) Absolute group velocity (the vector sum of U and C_{gr}, see Fig 1),

$$C_{ga} = (U^2 + C_{gr}^2 + 2U\ C_{gr}\ \text{Cos}(\delta - \alpha))^{1/2} \qquad\qquad 2.2.5$$

e) Ray direction (see Fig 1),

$$\mu = \tan^{-1} \left(\frac{U\ \text{Sin}\delta + C_{gr}\ \text{Sin}\alpha}{U\ \text{Cos}\delta + C_{gr}\ \text{Cos}\alpha}\right) \qquad\qquad 2.2.6$$

To derive kinematic quantities at the point under study (subscript i), given quantities at the previous point (subscript 0), Snell's law for the orthogonal direction, α, is used,

$$\text{Sin}\alpha_i = \frac{k_o}{k_i}\ \text{Sin}\alpha_o \qquad\qquad 2.2.7$$

This equation is used together with Equations 2.2.1-2.2.6 to predict all the kinematic quantities of interest at the point under study. These calculations are carried out separately for each wave component. The kinematic processes are linear, and do not involve the interaction of spectral components. A fuller discussion of current-depth refraction is given in Southgate (1985).

2.3 Wave statistics

Various spectrally averaged quantities are required both for calculation within the model and as output. Root-mean-square (rms) wave heights are calculated according to

$$H^2_{rms} = 8 \sum_\alpha \sum_\omega S_\zeta (\omega,\alpha) \; \Delta\omega \; \Delta\alpha \qquad\qquad 2.3.1$$

$$= \sum_\alpha \sum_\omega H^2_j \qquad\qquad 2.3.2$$

where $S_\zeta (\omega,\alpha)$ is the surface elevation spectral density for a particular angular wave frequency ω and direction α. $\Delta\omega$ and $\Delta\alpha$ are the band widths of the frequency and directional components. The subscript j denotes one spectral component.

The zero-crossing period (T_z) is calculated by,

$$T_z = 2\pi \left(\frac{\sum_\alpha \sum_\omega S_\zeta(\omega,\alpha) \; \Delta\omega \; \Delta\alpha}{\sum_\alpha \sum_\omega \omega^2 \; S_\zeta(\omega,\alpha) \; \Delta\omega \; \Delta\alpha} \right)^{\frac{1}{2}} \qquad\qquad 2.3.3$$

Average wave orthogonal directions are defined according to,

$$\bar{\alpha} = \tan^{-1} \left(\frac{\sum_\alpha \sum_\omega H^2_j \; Sin\alpha_j}{\sum_\alpha \sum_\omega H^2_j \; Cos\alpha_j} \right) \qquad\qquad 2.3.4$$

with a similar definition for average ray directions.

The rms bottom orbital velocity, V_{rms}, is calculated in the following way. The bottom orbital velocity spectral density, $S_u(\omega,\alpha)$ is related to the surface elevation spectral density according to,

$$S_u(\omega,\alpha) = S_\zeta(\omega,\alpha) \cdot \frac{\omega^2}{Sinh^2(kh)} \qquad \text{2.3.5}$$

V^2_{rms} is given by,

$$V^2_{rms} = \sum_\alpha \sum_\omega S_u(\omega,\alpha) \, \Delta\omega \, \Delta\alpha \qquad \text{2.3.6}$$

$$= \sum_\alpha \sum_\omega \frac{S_\zeta(\omega,\alpha) \, \omega^2}{Sinh^2(kh)} \Delta\omega \, \Delta\alpha \qquad \text{2.3.7}$$

or, since

$$H^2_j(\omega,\alpha) = 8 \, S_\zeta(\omega,\alpha) \, \Delta\omega \, \Delta\alpha, \qquad \text{2.3.8}$$

$$V^2_{rms} = \sum_\alpha \sum_\omega \frac{\omega^2 \, H^2_j(\omega,\alpha)}{8 \, Sinh^2(kh)} \qquad \text{2.3.9}$$

The O'Connor and Yoo (1988) boundary layer model is used to determine friction factors for wave and current energy dissipation by bottom friction. In this model the peak bottom orbital velocity of a monochromatic wave is used. For spectral waves, the peak value of the equivalent monochromatic wave (ie one with the same V_{rms} value) is substituted. Hence,

$$V_{peak} = \sqrt{2} \, V_{rms} \qquad \text{2.3.10}$$

giving

$$V^2_{peak} = \sum_\alpha \sum_\omega \frac{\omega^2 \, H^2_j(\omega,\alpha)}{4 \, Sinh^2(kh)} \qquad \text{2.3.11}$$

Similar calculations are performed for the semi-orbital excursion length, A, resulting in,

$$A^2_{rms} = \sum_\alpha \sum_\omega \frac{H^2_j(\omega,\alpha)}{8 \, Sinh^2(kh)} \qquad\qquad 2.3.12$$

and

$$A^2_{peak} = \sum_\alpha \sum_\omega \frac{H^2_j(\omega,\alpha)}{4 \, Sinh^2(kh)} \qquad\qquad 2.3.13$$

Using these quantities, a bottom velocity zero-crossing wave period, T_{zb}, can be defined by

$$T_{zb} = \frac{2\pi \, A_{rms}}{V_{rms}} \qquad\qquad 2.3.14$$

A mean bottom velocity direction is calculated by resolving each velocity spectral component in orthogonal directions. These can be arbitrarily chosen, but it is convenient to use the grid axes,

$$V^2_x = \sum_\alpha \sum_\omega \frac{\omega^2 \, H^2_j(\omega,\alpha)}{8 \, Sinh^2(kh)} Cos\alpha_j \qquad\qquad 2.3.15$$

$$V^2_y = \sum_\alpha \sum_\omega \frac{\omega^2 \, H^2_j(\omega,\alpha)}{8 \, Sinh^2(kh)} Sin\alpha_j \qquad\qquad 2.3.16$$

The mean bottom velocity direction, $\bar{\alpha}_b$, is then given by

$$\bar{\alpha}_b = tan^{-1} (V^2_y/V^2_x) \qquad\qquad 2.3.17$$

2.4 Wave dynamics

Determination of wave dynamic quantities (ie those related to the wave energy) is based on the equation of wave energy balance, or, more strictly speaking, the equation of wave action balance for each wave component,

$$\frac{d}{dy}\left(\frac{E\ C_{ga}\ Cos\mu}{\omega_r}\right) = -\frac{(D_f + D_b)}{\omega_r} \qquad 2.4.1$$

In this equation y is the coordinate in the onshore direction (Fig 1), E is the wave energy density per unit surface area, and D_f and D_b are the spatial energy dissipation rates due to seabed friction and wave breaking respectively. For each spectral component E is related to the wave height of that component by

$$E = \frac{1}{8}\rho g\ H^2 \qquad 2.4.2$$

in which ρ is the water density.

In the model, the wave height is determined by integrating Equation 2.4.1 and solving for H for each component separately. However, both seabed friction and wave breaking are non-linear processes and therefore the dissipation rate of the total spectrum has to be taken into account in the calculation of the dissipation rates of the individual components.

In Southgate (1987 and 1989), the wave energy dissipation rate for monochromatic waves was calculated using the formula

$$D_f = \rho\ C_{fw}\ V_o^3 \qquad 2.4.3$$

in which C_{fw} is the wave friction factor, enhanced by interaction with the current field, and V_o is the maximum wave orbital velocity at the seabed. V_o is related to the wave height by

$$V_o = \frac{H\ \omega_r}{2\ Sinh\ (kh)} \qquad 2.4.4$$

The determination of C_{fw} uses the boundary layer model of O'Connor and Yoo (1988). In the present method the rms bottom orbital velocity (Eq 2.3.9), bottom

zero-crossing period (Eq 2.3.14) and average bottom direction (Eq 2.3.17) are used in place of their equivalent monochromatic wave values in the O'Connor and Yoo boundary layer model.

Once the wave and current friction factors have been determined by the O'Connor and Yoo model, it is necessary to calculate the rate of dissipation of wave energy, D_f, under spectral waves, analogous to Equation 2.4.3 for monochromatic waves. The method of calculating D_f for spectral waves follows theory developed by Hasselmann and Collins (1968) and Collins (1972). Essentially, their method relies on the fact that the instantaneous work done by one wave component, W, is,

$$W = \underline{\tau} \cdot \underline{V} \qquad\qquad 2.4.5$$

in which $\underline{\tau}$ is the resultant bottom shear stress for the whole spectrum, and $\underline{V}$ is the bottom orbital velocity of one component. This leads to the following expression for the value of D_f for one spectral component (the subscript j denoting the jth component),

$$D_{fj}(\omega,\alpha) = (\frac{\pi}{2})^{\frac{1}{2}} \frac{\rho \; C_{fw} \; \omega^2}{4 \; Sinh^2 kh} \; H_j^2(\omega,\alpha) \cdot B_j(\omega,\alpha) \qquad 2.4.6$$

where $B_j(\omega,\alpha)$ is given by

$$B_j(\omega,\alpha) = p_1 + p_2 \; Cos^2(\alpha-\gamma) + p_3 \; Sin^2(\alpha-\gamma) \qquad 2.4.7$$

The angle γ is determine from the condition $\langle V_1 V_2 \rangle = 0$ in which V_1 is the component of bottom orbital velocity in the mean velocity direction, V_2 is the perpendicular component, and $\langle \; \rangle$ denotes mean

values averaged over all spectral components within a given spectrum. γ is explicitly determined from

$$Cos^4\gamma \ (f_3 - f_1)^2 + Cos^2\gamma \ (2f^2 - (f_3 - f_1)^2) - f_2^2 = 0$$

2.4.8

in which

$$f_1 = \sum_\alpha \sum_\omega H_j^2(\omega,\alpha) \ \frac{\omega^2}{8 \ Sinh^2kh} \ Cos^2\alpha_j$$

2.4.9

$$f_2 = \sum_\alpha \sum_\omega H_j^2(\omega,\alpha) \ \frac{\omega^2}{8 \ Sinh^2kh} \ Cos\alpha_j \ Sin\alpha_j$$

2.4.10

$$f_3 = \sum_\alpha \sum_\omega H_j^2(\omega,\alpha) \ \frac{\omega^2}{8 \ Sinh^2kh} \ Sin^2\alpha_j$$

2.4.11

Returning to Equation 2.4.7, p_1, p_2 and p_3 are given by,

$$p_1 = (\frac{2}{\pi})^{\frac{1}{2}} \ \sigma_1 \ E(m)$$

2.4.12

$$p_2 = (\frac{2}{\pi})^{\frac{1}{2}} \ \sigma_1 \ [\frac{E(m)}{m^2} - \frac{K(m)}{m^2} (1 - m^2)]$$

2.4.13

$$p_3 = (\frac{2}{\pi})^{\frac{1}{2}} \ \sigma_1 \ [\frac{(1 - m^2) \ (K(m) - E(m))}{m^2}]$$

2.4.14

in which

$$\sigma_1^2 = f_1 \ Cos^2\gamma + 2f_2 \ Cos\gamma \ Sin\gamma + f_3 \ Sin^2\gamma$$

2.4.15

$$\sigma_2^2 = f_1 \ Sin^2\gamma - 2f_2 \ Cos\gamma \ Sin\gamma + f_3 \ Cos^2\gamma$$

2.4.16

$$m = (1 - \sigma_2^2 / \sigma_1^2)^{\frac{1}{2}}$$

2.4.17

and K(m) and E(m) are complete elliptic integrals of the first and second kinds respectively.

The method of modelling energy dissipation by wave breaking is based on the theory of Battjes and Janssen (1978). These authors modelled the energy dissipated by breaking waves using an expression originally derived for a tidal bore, a phenomenon similar in appearance to a broken wave. Their analysis resulted in the following expression for the spatial rate of total energy dissipation (D_b) in a random wave field,

$$D_b = \frac{\lambda \rho g^{3/2} k H_{rms}^3 f(Q)}{8\pi h^{1/2}}$$ 2.4.18

in which λ is an empirical factor, close to one, expressing the difference between the wave breaking and tidal bore processes. Q is the probability of occurrence of broken waves determined by Battjes and Janssen assuming a Rayleigh distribution of wave heights, as

$$\frac{1 - Q}{(- \ln Q)} = (\frac{H_{rms}}{H_b})^2$$ 2.4.19

This is an implicit equation for Q in terms of H_{rms} and the breaker wave height, H_b. f(Q) in Equation 2.4.18 is given by

$$f(Q) = Q(\frac{- \ln Q}{1 - Q})^{3/2}$$ 2.4.20

The breaker height, H_b, is calculated by the empirical formula put forward by Weggel (1972) and recommended by the American Shore Protection Manual,

$$H_b = \frac{ah}{1 + bh/(gT^2)}$$ 2.4.21

in which

$$a = \frac{2a'}{1 + \exp(-19.5s)}$$ 2.4.22

$$b = 43.75 \ (1 - \exp(-19s))$$ 2.4.23

s is the seabed slope, T is the wave period, and a' is an empirically determined parameter (see Section 3.2.2).

Equation 2.4.18 determines the breaking energy dissipation rate of the total wave field. In the present model, in which wave spectra are considered, some assumption has to be made about the distribution of energy loss over the spectral components. The plausible assumption is made that the energy dissipation rate of each component is proportional to the pre-breaking energy in that component. In other words, if H_j is the wave height of the jth spectral component, the dissipation rate (D_{bj}) for that component is

$$D_{bj} = D_b \cdot \frac{H_j^2}{H_{rms}^2}$$ 2.4.24

or, from Equation 2.4.18,

$$D_{bj} = \frac{\lambda \ \rho \ g^{3/2} \ k \ H_{rms} \ H_j^2 \ f(Q)}{8\pi h^{1/2}}$$ 2.4.25

Having obtained explicit expressions for D_{fj} and D_{bj}, it is now possible to integrate the wave action balance equation (Eq 2.4.1) separately for each spectral component. This method is identical to that for monochromatic waves (Southgate 1988 and 1989), and the result is

11

$$H_i = H_o \, K_s \, K_r \, K_d \, \frac{1}{1 + \beta H_o} \qquad\qquad 2.4.26$$

in which the subscript i denotes predicted values at the grid point under study, and o denotes known values at the previous grid point. The other quantities are:

$$K_s = (\frac{C_{gao}}{C_{gai}})^{\frac{1}{2}} \qquad \text{Shoaling Coefficient} \qquad 2.4.27$$

$$K_r = (\frac{\cos \mu_o}{\cos \mu_i})^{\frac{1}{2}} \qquad \text{Refraction Coefficient} \qquad 2.4.28$$

$$K_d = (\frac{\omega_{ri}}{\omega_{ro}})^{\frac{1}{2}} \qquad \text{Doppler Coefficient} \qquad 2.4.29$$

$$\beta = \frac{1}{2} (\frac{C_{gao} \cos \mu_o}{\omega_{ro}})^{\frac{1}{2}} \int_{y_o}^{y_i} (\frac{\omega_r}{C_{ga} \cos \mu})^{3/2} [\frac{C_{fw} \, \omega_r^2}{g \, \sinh^3(kh)} + \frac{\lambda \, g^{\frac{1}{2}} \, k \, f(Q)}{\pi \, \omega_r \, h^{\frac{1}{2}}}] \, dy$$

$$2.4.30$$

The integral in Equation 2.4.30 is evaluated numerically by the trapezium rule. An iterative procedure is used to improve the calculation of β and H_i (Southgate 1988). Once H_i has been calculated for each spectral component, the root-mean-square wave height is determined by

$$H_{rms} = (\sum_j H_{ij}^2)^{\frac{1}{2}} \qquad\qquad 2.4.31$$

2.5 Wave radiation stresses

The onshore (S_{yy}) and longshore (S_{xy}) components of the wave radiation stress are evaluated separately for each spectral wave component according to:

$$S_{yy} = \frac{1}{8} \rho g \; H^2 \; [(\frac{2 \; C_{gr}}{C_r} - \tfrac{1}{2}) \; Cos^2\alpha + (\frac{C_{gr}}{C_r} - \tfrac{1}{2}) \; Sin^2\alpha]$$

<div align="right">2.5.1</div>

$$S_{xy} = \frac{\rho g \; H^2 \; C_{gr} \; Sin2\alpha}{16C_r}$$

<div align="right">2.5.2</div>

A simplification in the calculation of S_{xy} is made using the fact that the irrotational part of S_{xy} remains unaltered by the process of current-depth refraction for the 1-D approximation used in the model. The only changes to S_{xy} are by the dissipative processes of bottom friction and wave breaking. It was shown in Southgate (1987) that the change in wave radiation stress between grid points is given by

$$S_{xyi} = \frac{S_{xyo}}{(1 + \beta H_o)^2}$$

<div align="right">2.5.3</div>

After summation over the S_{yy} components, the wave-induced set-up is calculated from the momentum balance equation in the onshore direction,

$$\frac{d\eta}{dy} = - \frac{1}{\rho g \; (h + \eta)} \; \frac{d}{dy} \; (\sum_{j} S_{yy})$$

<div align="right">2.5.4</div>

in which η is the set-up of the still water level. A finite difference formulation of Equation 2.5.4 gives

$$\eta_i = - h + [(h + \eta_o)^2 - \frac{2 \; \Delta S_{yy}}{\rho g}]^{\frac{1}{2}}$$

<div align="right">2.5.5</div>

in which

$$h = (h_i + h_o)/2$$

<div align="right">2.5.6</div>

and $\Delta S_{yy} = (\sum_j S_{yy})_i - (\sum_j S_{yy})_o$ 2.5.7

The gradient of S_{xy} in the y-direction provides the driving force for the longshore wave-induced current. The value of this force per unit sea area (F) is

$$F = - \frac{d}{dy} (\sum_j S_{xy}) \qquad\qquad 2.5.8$$

The technique of current modelling is identical to that used in the monochromatic wave version of the model. Details of this method are given in Southgate (1988 and 1989).

3 COMPARISON BETWEEN SPECTRAL AND MONOCHROMATIC WAVES

3.1 Introduction

In Southgate (1988 and 1989), the monochromatic wave version of the Nearshore Profile Model was compared with the laboratory data of Visser (1984a and 1984b). In order to discover the effects of spectral wave propagation, compared with the equivalent monochromatic wave, these tests were repeated in the Nearshore Profile Model using two frequency spectra of different types, a Top-Hat (ie a truncated white noise) spectrum and a Pierson-Moskowitz spectrum. These frequency spectra were run separately with monodirectional waves and with a $Cos^6(\alpha-\bar{\alpha})$ directional spectrum. In each case the spectra were chosen such that the initial H_{rms}, T_z and $\bar{\alpha}$ values corresponded to the initial H, T and α values used in the monochromatic wave tests. After these tests, a further comparison of spectral and monochromatic waves was carried out using typical field data, again with Top-Hat and Pierson-Moskowitz frequency spectra and

$Cos^6(\alpha-\bar{\alpha})$ directional spectra.

3.2 Tests using Laboratory Data

3.2.1 Experimental arrangement

Visser's experimental arrangement consisted of a 2-D flat wave basin with a regular slope up to a beach at one end, and no lateral variation of depth. Monochromatic waves were generated with a snake-type generator, capable of creating long-crested waves at an angle to the generator. Diffraction effects at the ends of the generator were minimised by the use of waveguides. An important feature of Visser's experiments was the careful use of a distribution system to prevent end effects from contaminating the longshore currents created when the waves break. The basin layout is shown in Figure 2 and is described in detail in Visser (1984a and 1984b).

Three tests were carried out with a bed slope of 1 in 10, and four with a slope of 1 in 20. Different input wave conditions or bed roughnesses were used in each test. For the present comparison between spectral and monochromatic wave predictions, results from the first of these seven tests were used. This test was carried out with a smooth concrete bed with a beach slope of 1 in 10 and a surface roughness of 0.2mm.

3.2.2 Incident Wave Conditions

The incident wave conditions for the experimental tests were:

Wave height = 0.072m

Wave period = 2.01s

Wave direction = 31.1° (angle between forward
ray direction and profile line).

A run of the Nearshore Profile Model was carried out
using monochromatic waves with these values of the
input parameters. The run was then repeated using
four different types of incident wave spectrum. These
consisted of

a)   A Pierson-Moskowitz frequency spectrum and
     $\cos^6(\alpha-\bar{\alpha})$ directional spectrum.
b)   A Pierson-Moskowitz frequency spectrum and
     monodirectional waves.
c)   A Top-Hat frequency spectrum and $\cos^6(\alpha-\bar{\alpha})$
     directional spectrum.
d)   A Top-Hat frequency spectrum and monodirectional
     waves.

Six bands for the Pierson-Moskowitz spectrum were used
(with equal increments in period) and seven for the
Top-Hat spectrum. The directional spectrum had nine
angular bands. The spectral densities (and therefore
the wave energies) associated with each band were
chosen so that the spectrally averaged incident values
of wave height, period and direction matched the
values used in the Visser tests. Table 1 shows these
incident wave conditions and spectral band widths for
each spectrum. The notation F6D9 refers to full
spectral runs (six frequency bands and nine
directional bands), F6D1 to frequency spectra only,
and F1D1 to monochromatic waves. F7D9 and F7D1 are
similarly defined.

At each grid point on the profile line, comparisons
were made between each model run of three parameters,

the longshore current velocity, the wave set-up and the wave height (an rms value in the case of spectral runs).

It was found in earlier tests that the calculation of longshore current velocities and wave set-up required a different input value of the breaker parameter, a', for the calculation of wave heights in the breaker zone. The reason is that the breaking process starts to affect wave heights at the breaker point, where the wave crest initially begins to curl over, whereas longshore currents and wave set-up are not affected until the plunge point is reached, where the crest strikes the still water in front of the wave. This consideration only applies to plunging breakers, which were the type occurring in the physical model. Accordingly the full set of runs was carried out using two different values of a',

a' = 1.18. Tuning to the plunge line for calculation of longshore currents and wave set-up.

a' = 0.78. Tuning to the breaker line for calculation of wave heights.

3.2.3 Results

The results are presented as plots of wave height, wave set-up and wave-induced longshore current velocity against offshore direction from the intersection of the still water line with the beach. Figures 3-8 show two sets of plots, for the Pierson-Moskowitz and Top-Hat spectra. Each figure shows four cases, outlined below:

<u>Figures 3,4,5</u>

a)   NPM, P-M frequency spectrum, $\cos^6(\alpha-\bar{\alpha})$
     directional spectrum
b)   NPM, P-M frequency spectrum, monodirectional
     waves
c)   NPM, Monochromatic waves
d)   Physical model, Monochromatic waves.

<u>Figures 6,7,8</u>

a)   NPM, Top-Hat frequency spectrum, $\cos^6(\alpha-\bar{\alpha})$
     directional spectrum
b)   NPM, Top-Hat frequency spectrum, monodirectional
     waves
c)   NPM, Monochromatic waves
d)   Physical model, Monochromatic waves.

Figures 3 and 6 show longshore current velocities,
Figures 4 and 7 show water set-up, and Figures 5 and 8
show wave heights (rms values for the spectral runs).

The following observations can be made on these
figures:

a)   Longshore current velocities (Figs 3 and 6).

Seawards of the breaking region (ie where the peak
occurs), there is little difference between the
spectral (F6D9) and monochromatic (F1D1) runs. At the
peak, there is a significant difference between the
two of about 20%. The difference is considerably
greater in going from F6D1 to F6D9 than from F1D1 to
F6D1, indicating that the effect of a directional
spectrum is more significant than a frequency
spectrum. The effects of the Top-Hat spectrum are

slightly stronger than the Pierson-Moskowitz spectrum, as would be expected since the Top-Hat spectrum contains greater amounts of wave energy away from the mean frequency. The agreement with experimental data is better for F1D1 than F6D9 for both types of frequency spectra.

b)   Wave set-up (Figs 4 and 7)

Differences between the spectral (F6D9) and monochromatic (F1D1) runs are insignificant seaward of the breaker region (where the minimum occurs). Differences occur in the wave set-up landwards of the breaker region, with the greatest set-up for F1D1. In contrast to the longshore current velocities, there is a somewhat larger effect in going from F1D1 to F6D1 than from F6D1 to F6D9. There is little difference between the Top-Hat and Pierson-Moskowitz spectra, and the F1D1 results do not appear to give significantly better agreement with experimental data than the spectral runs.

c)   Wave Heights (Figs 5 and 8)

The effect of including wave spectra is to reduce the wave heights by a maximum of about 7%. The largest effect occurs in going from F7D9 to F7D1, indicating that directional spreading of wave energy is more important than frequency spreading. The differences between results using the Pierson-Moskowitz spectrum and the Top-Hat spectrum are very small. In all of these tests the wave breaking process is treated as applying to random waves (including F1D1, where all other processes are regarded as applying to monochromatic waves). If the breaking process is additionally regarded as applying to monochromatic

19

waves, considerably better agreement with the experimental data is obtained (see Fig 31 of Southgate 1988).

3.3 Tests using Field Data

3.3.1 Introduction and Model Set-up

In the Spring of 1987, Hydraulics Research carried out a field measurement exercise in the area around Aberdeen Harbour. As part of this exercise, tidal current velocities were measured using float-tracking drogues released from various points along a shore-normal line just north of the harbour (Fig 9). These measurements were subsequently used to test the Nearshore Profile Model in its predictions of tidal current velocities (Southgate 1988 and 1989).

For the present purpose, the same model set-up, profile line and bathymetry were used to assess the relative effects of spectral and monochromatic waves in a field situation. The profile line consisted of 41 grid points extending from deep water (50m CD) to the top of the beach. The grid points were not evenly spaced, being more concentrated nearer the coastline. Sediment samples from the site indicated a seabed composed predominantly of fine to medium sand (about 200 microns). Accordingly the bed roughness factor was set to a value appropriate to a typical ripple height for this type of sand, of 0.016m.

For running the model with monochromatic waves the following input wave parameters were used,

H = 2.5m

T = 8.0s

α = 30° (angle between forward ray direction and profile line).

Top-Hat and Pierson-Moskowitz frequency spectra were then constructed to give the same mean values of H_{rms} and T. The band widths and wave energies in each band are shown in Table 2. A $Cos^6(\alpha-\bar{\alpha})$ directional spectrum was used.

3.3.2 Results

Three sets of runs were carried out using

a) Pierson-Moskowitz frequency spectrum and $Cos^6(\alpha-\bar{\alpha})$ directional spectrum

b) Top-Hat frequency spectrum and $Cos^6(\alpha-\bar{\alpha})$ directional spectrum

c) Monochromatic waves.

Figures 10, 11 and 12 show respectively the longshore current velocity, wave set-up and wave heights (rms values for the spectral runs) for the portion of the profile line around the breaker zone, extending to 660m seawards from the shoreline.

The following observations are made on the figures.

a) Longshore Current Velocities (Fig 10)

There is little difference between results for the two types of spectra but a considerable difference between these and the monochromatic run. At the peak velocity this difference is about 20%, similar to that found in the laboratory comparison. Shorewards of the breaker zone the monochromatic values are consistently higher than the spectral values, but seawards they become smaller.

b) Wave Set-up (Fig 11)

Seawards of the breaker zone, differences between the
runs are insignificant. Landwards, the monochromatic
run initially gives the highest set-up, the but very
close to the coast the highest values are achieved by
the Top-Hat spectrum. It would appear that the amount
of wave set-up is largely dependent on the details of
the spectrum.

c) Wave Heights (Fig 12)

Differences of about 7% in wave height occur between
the monochromatic run and the Pierson-Moskowitz
spectrum around the breaker zone, a similar value to
that found in the laboratory tests. In contrast to
those tests, however, the Top-Hat spectrum values are
much closer to the monochromatic values. Close to the
coast the Top-Hat values actually exceed the
monochromatic values.

4 CONCLUSIONS

For the prediction of wave set-up, the "equivalent
monochromatic wave" assumption appears to provide
sufficiently accurate results as those using a full
frequency and directional spectrum. For the
prediction of wave heights, this assumption results in
an overprediction by up to about 7%. This is on the
borderline of acceptable accuracy for most
applications and therefore it is recommended that for
the prediction of wave heights the model should be
used with full input spectra where these are
accurately known. However, the equivalent
monochromatic wave assumption gives higher, and
therefore conservative, wave heights. This assumption
would therefore be justified if the incident spectra
were not known, or known only with poor accuracy. For
applications involving the analysis of tens or

22

hundreds of thousands of wave values (for instance to provide a data set for statistical extrapolation to extreme wave heights) the use of monchromatic waves may also be justified if there is a limit on the available computing time.

For longshore current velocities, the equivalent monochromatic wave can overpredict by up to 20%. In applications to longshore sediment transport this factor will be further increased. Assuming that sediment transport rates obey a fourth-power law in current velocity, at 20% difference in current velocity will result in a doubling of the sediment transport rate. However, this apparently large difference is still relatively small when set against a variety of factors which contribute to the generally poor predictions of sediment transport rates using presently available theoretical and empirical formulae.

Overall it is recommended that spectral waves should be used in the Nearshore Profile Model where these are reasonably accurately known and when it is feasible in terms of computational effort. If very large numbers of wave conditions are required it may be necessary to coarsen the spectral matrix or even to use the equivalent monochromatic wave if computational time and cost are limiting factors. However, it is anticipated that under most circumstances, spectral wave input can be used.

REFERENCES

1. BATTJES J A and JANSSEN J P F M, "Energy loss and set-up due to breaking of random waves", Proc. 16th International Conference on Coastal Engineering, ASCE, Hamburg pp 569-587, 1978.

2. COLLINS J I, "Prediction of shallow-water spectra", J. Geophys. Res., Vol 77, No 15, pp 2693-2707, 1972.

3. HASSELMANN K and COLLINS J I, "Spectral dissipation of finite-depth gravity waves due to turbulent bottom friction", J. Marine Res., Vol 26, No 1, pp 1-12, 1968.

4 O'CONNOR B A and YOO D, "Mean bed friction of combined wave-current flow", Coastal Engineering, Vol 12, No 1, March 1988.

5. SOUTHGATE H N, "Current-depth refraction of water waves. A description and verification of three numerical models", Report SR 14, Hydraulics Research Ltd, January 1985.

6. SOUTHGATE H N, "A one-dimensional model of wave-current interaction", ASCE Speciality Conference on Coastal Hydrodynamics, Delaware, USA, 1987.

7. SOUTHGATE H N, "The nearshore profile model", Report SR 157, Hydraulics Research Ltd, February 1988.

8. SOUTHGATE H N, "A nearshore profile model of wave and tidal current interaction", Coastal Engineering, 1989 (to appear).

9. VISSER P J, "A mathematical model of the uniform longshore currents and the comparison with laboratory data", Report No 84-2, Dept. of Civil Eng., Delft Univ. of Tech., 1984a.

10. VISSER P J, "Uniform longshore current measurements and calculations", 19th International Conference on Coastal Engineering, ASCE, Houston, USA, 1984b.

11. WEGGEL J R, "Maximum breaker height", J. Waterways, Harbours and Coastal Eng. Div., ASCE, Vol 98, 1972.

LIST OF SYMBOLS

a	Wave breaking parameter, Eq 2.4.22
a'	Wave breaking parameter, Eq 2.4.22
A	Wave semi-orbital excursion length at seabed
A_{rms}	Root-mean-square value of A for wave spectrum, Eq 2.3.9
A_{peak}	Peak value of A for wave spectrum, Eq 2.3.10
b	Wave breaking parameter, Eq 2.4.23
B	Defined by Eq 2.4.7
C_{fw}	Wave friction factor
C_{ga}	Absolute wave group velocity, Eq 2.2.5
C_{gr}	Relative wave group velocity, Eq 2.2.4
C_r	Relative wave celerity, Eq 2.2.3
D_f	Rate of dissipation of wave energy by seabed friction
D_b	Rate of dissipation of wave energy by breaking
E	Wave energy density per unit surface area
$E(m)$	Complete elliptic integral of the second kind
f	Absolute wave frequency
f_1	Defined by Eq 2.4.9
f_2	Defined by Eq 2.4.10
f_3	Defined by Eq 2.4.11
$f(Q)$	Defined by Eq 2.4.20
F	Force per unit surface area in longshore direction exerted by radiation stress, Eq 2.5.8
g	Acceleration due to gravity
h	Water depth
H	Wave height
H_b	Breaker wave height
H_{rms}	Root-mean-square wave height
k	Wavenumber, Eq 2.2.1
K_d	Doppler coefficient, Eq 2.4.29
K_r	Refraction coefficient, Eq 2.4.28
K_s	Shoaling coefficient, Eq 2.4.27
$K(m)$	Complete elliptic integral of the first kind
m	Defined by Eq 2.4.17
p_1	Defined by Eq 2.4.12
p_2	Defined by Eq 2.4.13
p_3	Defined by Eq 2.4.14

26

Q	Probability of occurrence of broken waves, Eq 2.4.19
s	Seabed slope
S or S_ζ	Surface elevation spectral density
S_u	Bottom orbital velocity spectral density
S_{xy}	Longshore component of wave radiation stress, Eq 2.5.2
S_{yy}	Onshore component of wave radiation stress, Eq 2.5.1
T	Wave period
T_z	Zero-crossing wave period, Eq 2.3.3
T_{zb}	Zero-crossing wave period at the seabed, Eq 2.3.14
U	Depth-averaged current velocity
V	Wave bottom orbital velocity for monochromatic waves
V_o	Peak wave bottom orbital velocity for monochromatic waves
V_{peak}	Peak wave bottom orbital velocity for spectral waves, Eq 2.3.11
V_{rms}	Root-mean-square wave bottom orbital velocity for spectral waves, Eq 2.3.9
V_x	x-component of V_{rms}, Eq 2.3.15
V_y	y-component of V_{rms}, Eq 2.3.16
W	Instantaneous work on seabed done by one wave component, Eq 2.4.5
x	Co-ordinate in longshore direction
y	Co-ordinate in onshore direction
α	Wave orthogonal direction
$\bar{\alpha}$	Average wave orthogonal direction for spectral waves, Eq 2.3.4
$\bar{\alpha}_b$	Average wave bottom velocity direction for spectral waves, Eq 2.3.17
β	Wave dissipation factor, Eq 2.4.30
γ	Defined by Eq 2.4.8
δ	Current direction
η	Wave set-up
λ	Wave breaking parameter, Eq 2.4.18
μ	Wave ray direction, Eq 2.2.6
ρ	Water density
σ_1	Defined by Eq 2.4.15
σ_2	Defined by Eq 2.4.16
$\sum$	Summation sign

ω_a Absolute angular wave frequency (= $2\pi f$)

ω_r Relative angular wave frequency, Eq 2.2.2

Subscripts

o	Previous grid point
i	Present grid point
j	Individual wave spectral components
x	Component in x-direction
y	Component in y-direction

Abbreviations

F7D9	Wave spectrum with seven frequency bands and nine directional bands. Similar definitions apply to different numbers
F1D1	Monochromatic wave
Monochromatic	Monofrequency and monodirectional wave
NPM	Nearshore Profile Model
P-M	Pierson-Moskowitz
rms	Root-mean-square
1-D	One-dimensional

TABLES.

TABLE 1   Incident Spectra for Laboratory Tests

1. Frequency Spectra

a) Pierson-Moskowitz (H_{rms} = 7.2cm, Peak period = 2.0s)

Period range (sec)	0.25 to 0.75	0.75 to 1.25	1.25 to 1.75	1.75 to 2.25	2.25 to 2.75	2.75 to 3.25
Central period value (T) (sec)	0.5	1.0	1.5	2.0	2.5	3.0
$\Delta f = \Delta T/T^2$	2.0	0.5	0.2222	0.125	0.08	0.05556
$S(f)\Delta f = H^2/8$ (x10^{-6}) (m²s)	12.38	92.18	226.14	233.79	78.08	5.44

b) Top-Hat (H_{rms} = 7.2cm, Peak Period = 2.0s)

Period range (sec)	0.25 to 0.75	0.75 to 1.25	1.25 to 1.75	1.75 to 2.25	2.25 to 2.75	2.75 to 3.25	3.25 to 3.75
Central period value (T) (sec)	0.5	1.0	1.5	2.0	2.5	3.0	3.5
$\Delta f = \Delta T/T^2$	2.0	0.5	0.2222	0.125	0.08	0.05556	0.04082
$S(f) \Delta f = H^2/8$ (x10^{-6}) (m²s)	92.57	92.57	92.57	92.57	92.57	92.57	92.57

2. Directional Spectra

Range relative to $\bar{\alpha}$ = 0 (degrees)	-45 to -35	-35 to -25	-25 to -15	-15 to -5	-5 to 5	5 to 15	15 to 25	25 to 35	35 to 45
Central value (degrees)	-40	-30	-20	-10	0	10	20	30	40
$\cos^6(\alpha-\bar{\alpha})$ normalised to one	0.0244	0.0652	0.1252	0.1822	0.2060	0.1822	0.1252	0.0652	0.0244

$\bar{\alpha}$ is at an angle of 31.1 degrees to the profile line.

TABLE 2 Incident Spectra for Field Tests

1. Frequency Spectra

a) Pierson-Moskowitz (H_{rms} = 2.5m, Peak period = 8.0s)

Period range (sec)	2.5 to 3.5	3.5 to 4.5	4.5 to 5.5	5.5 to 6.5	6.5 to 7.5	7.5 to 8.5	8.5 to 9.5	9.5 to 10.5	10.5 to 11.5	11.5 to 12.5	12.5 to 13.5
Central period value (T) (sec)	3.0	4.0	5.0	6.0	7.0	8.0	9.0	10.0	11.0	12.0	13.0
$\Delta f = \Delta T/T^2$	0.11111	0.0625	0.04	0.02778	0.02041	0.01563	0.01235	0.01	0.00826	0.00694	0.00592
$S(f)\Delta f = H^2/8$ (x10⁻³) (m²s)	25.41	57.10	99.65	140.31	159.03	141.51	94.96	45.23 ✓	14.73	2.98	0.35

b) Top-Hat (H_{rms} = 2.5m, Peak Period = 8.0s)

Period range (sec)	2.5 to 3.5	3.5 to 4.5	4.5 to 5.5	5.5 to 6.5	6.5 to 7.5	7.5 to 8.5	8.5 to 9.5	9.5 to 10.5	10.5 to 11.5	11.5 to 12.5	12.5 to 13.5
Central period value (T) (sec)	3.0	4.0	5.0	6.0	7.0	8.0	9.0	10.0	11.0	12.0	13.0
$\Delta f = \Delta T/T^2$	0.11111	0.0625	0.04	0.02778	0.02041	0.01563	0.01235	0.01	0.00826	0.00694	0.00592
$S(f) \Delta f = H^2/8$ (x10⁻³) (m²s)	71.02	71.02	71.02	71.02	71.02	71.02	71.02	71.02	71.02	71.02	71.02

2. Directional Spectra

Range relative to $\bar{\alpha}$ = 0 (degrees)	-55 to -45	-45 to -35	-35 to -25	-25 to -15	-15 to -5	-5 to 5	5 to 15	15 to 25	25 to 35	35 to 45	45 to 55
Central value (degrees)	-50	-40	-30	-20	-10	0	10	20	30	40	50
$\cos^6(\alpha-\bar{\alpha})$ normalised to one	0.0059	0.0241	0.0644	0.1237	0.1801	0.2036	0.1801	0.1237	0.0644	0.0241	0.0059

$\bar{\alpha}$ is at an angle of 30.0 degrees to the profile line.

FIGURES.
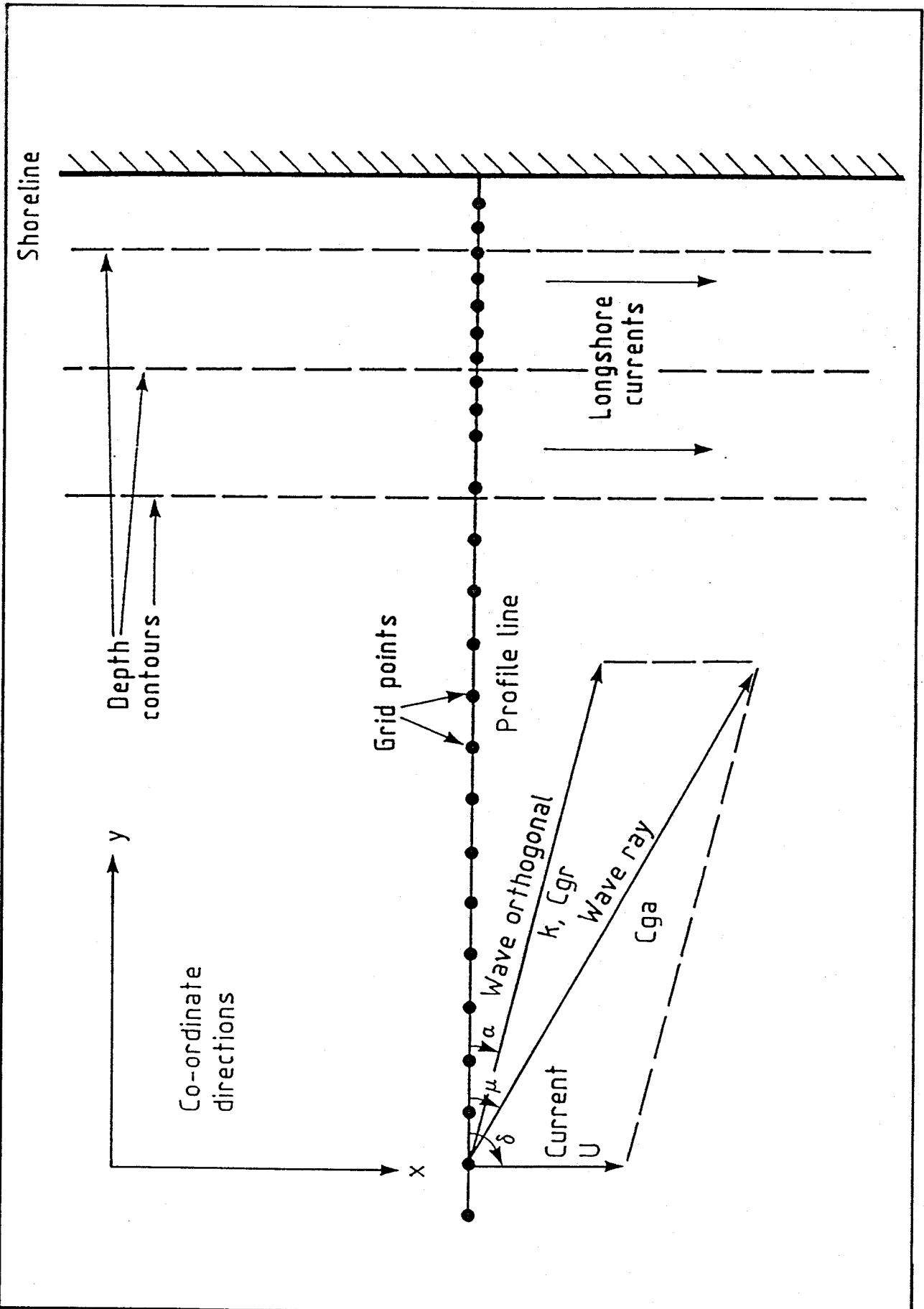
Fig 1   Model geometry of the Nearshore region
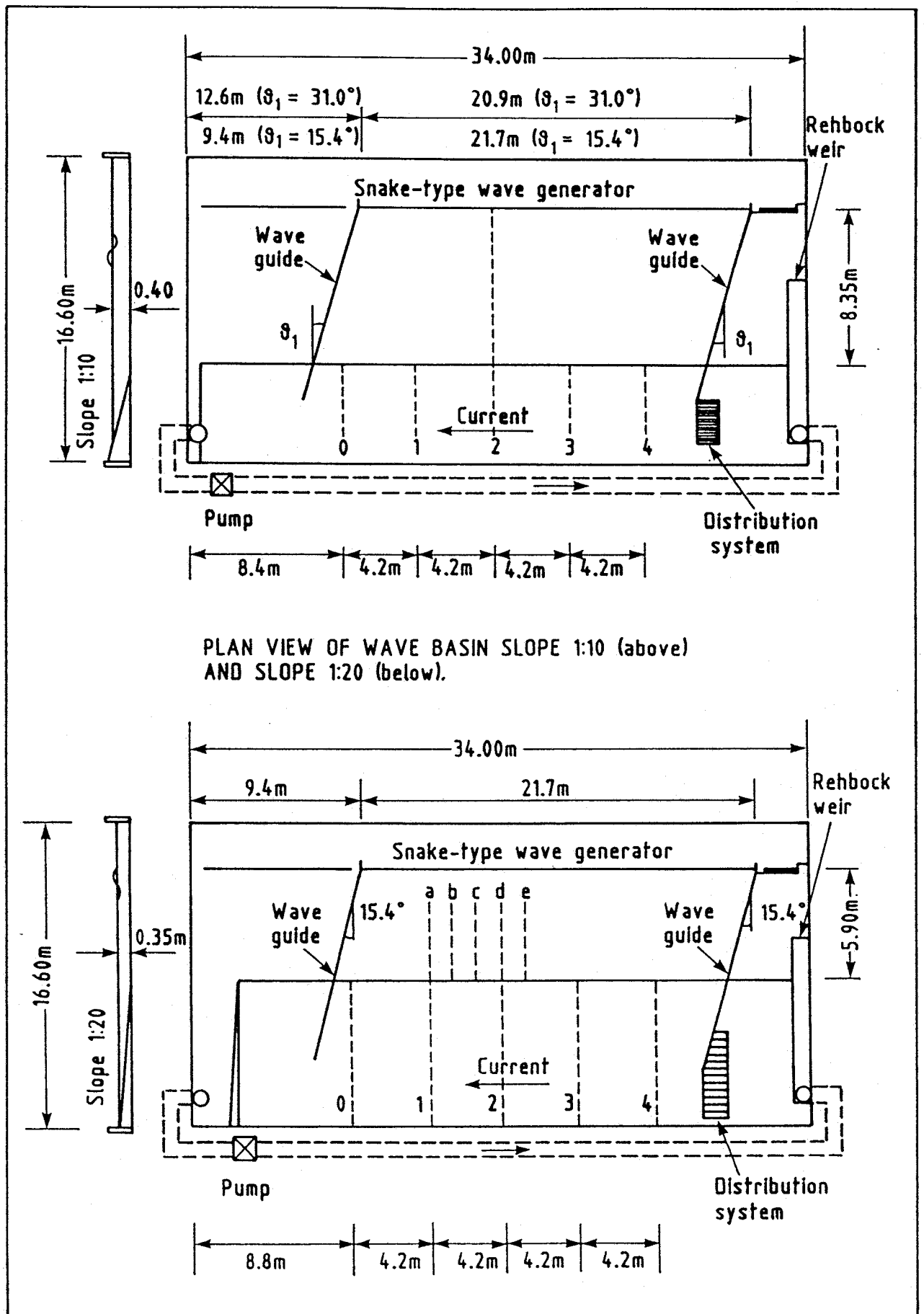
Fig 2   Experimental arrangement used by Visser (from Visser (1984a))
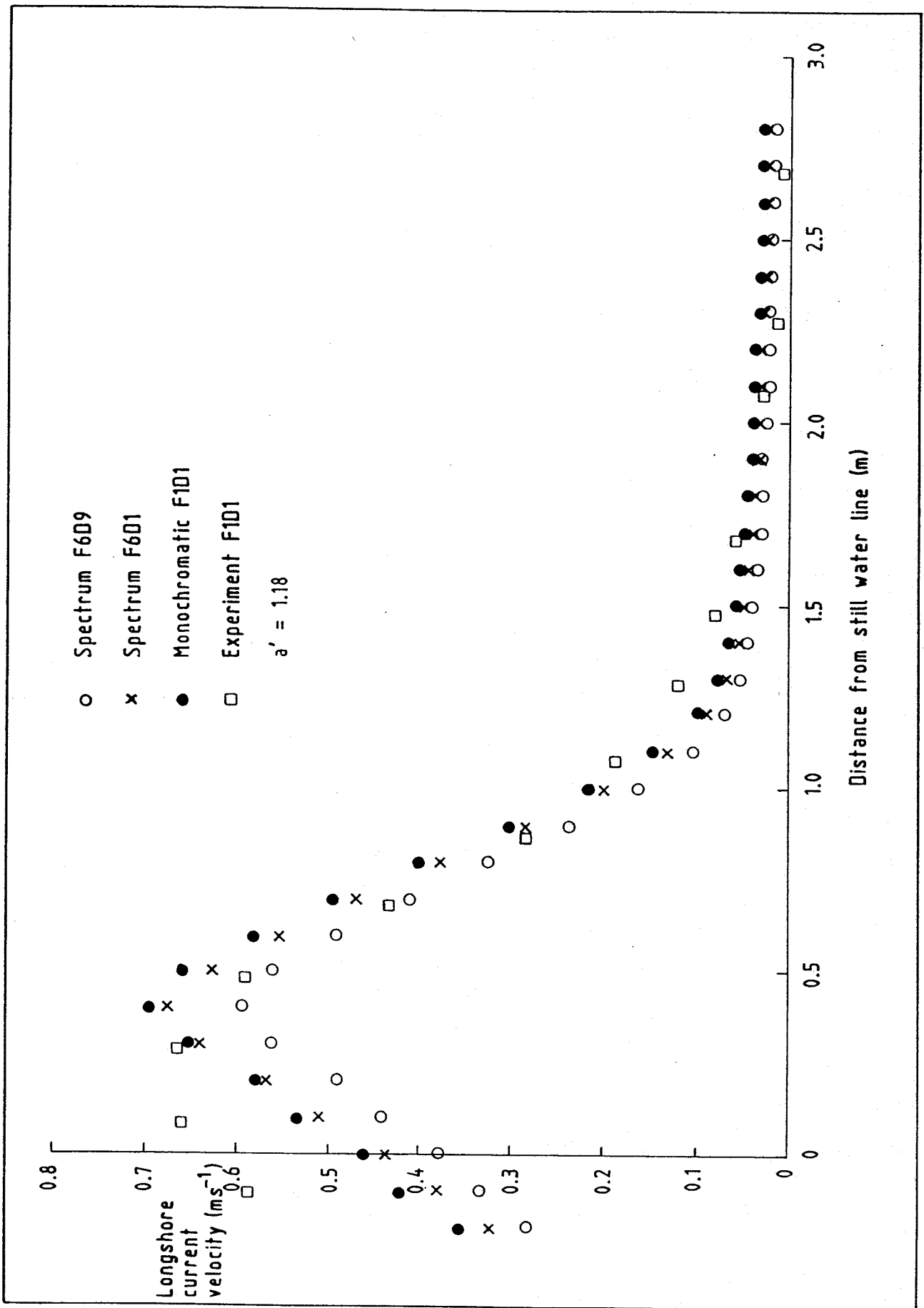
Fig 3   Laboratory tests – Pierson-Moskowitz spectrum – longshore current velocities
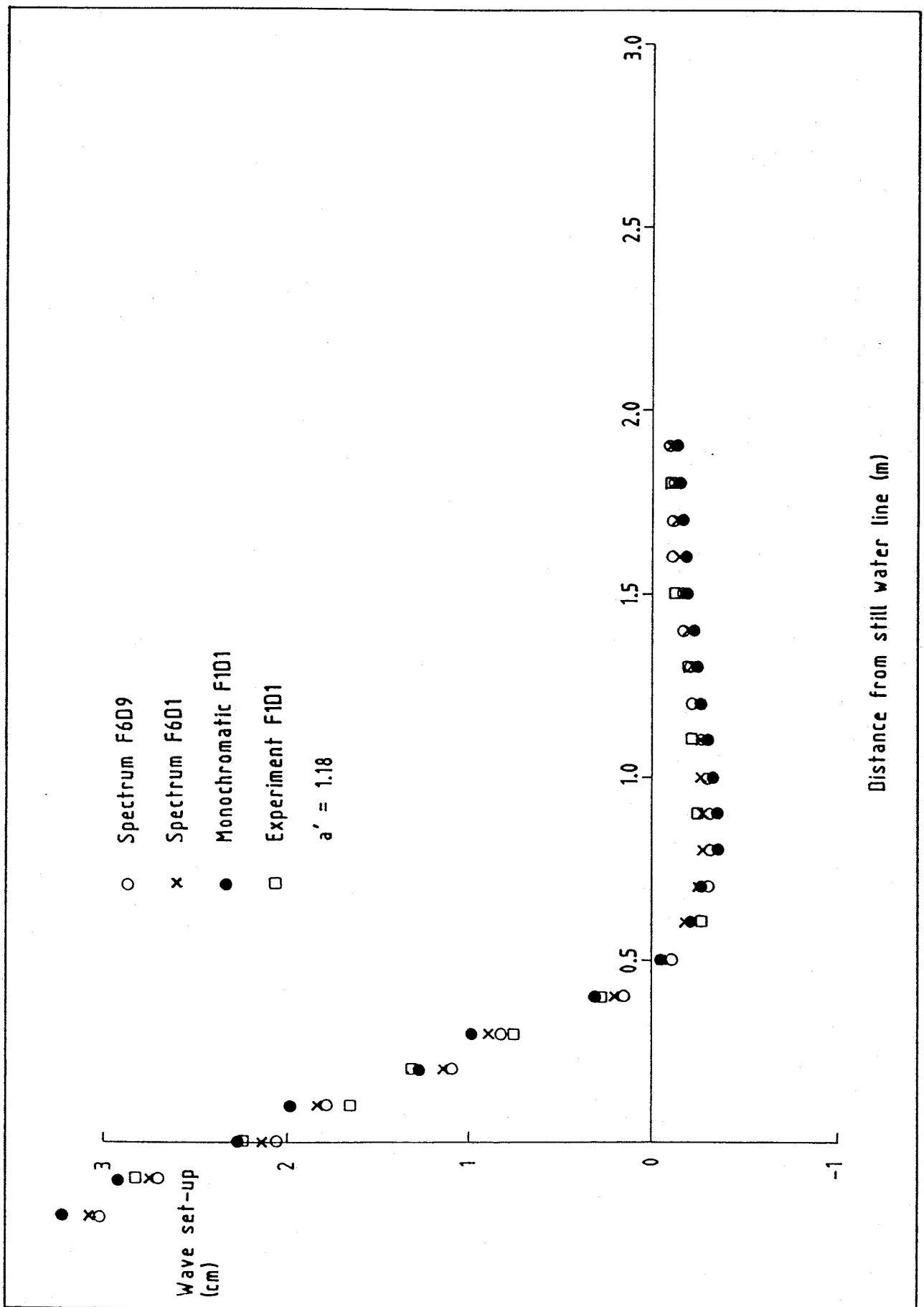
Fig 4   Laboratory tests – Pierson-Moskowitz spectrum – wave set-up
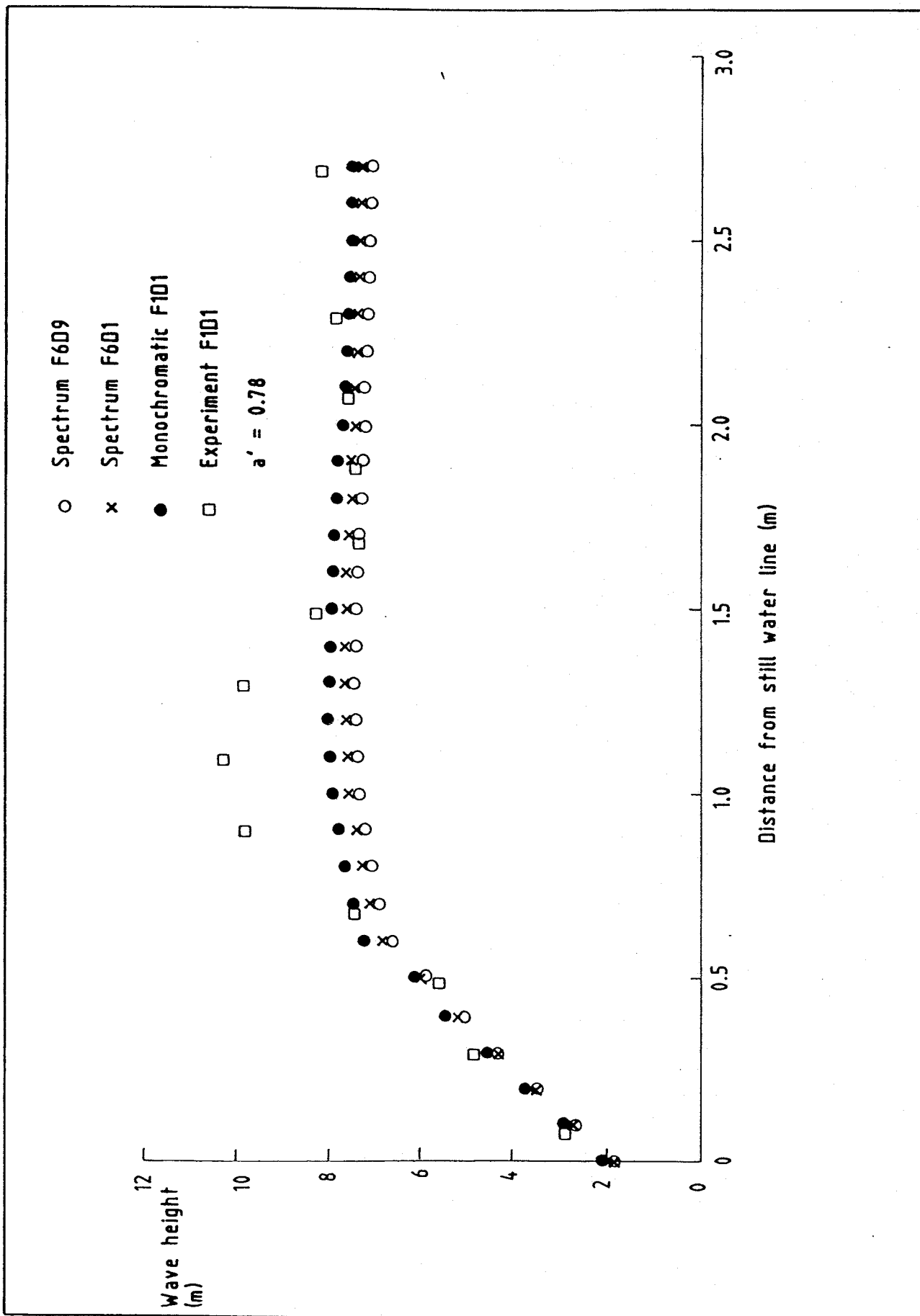
Fig 5 Laboratory tests – Pierson–Moskowitz spectrum – wave heights (RMS values for spectra).
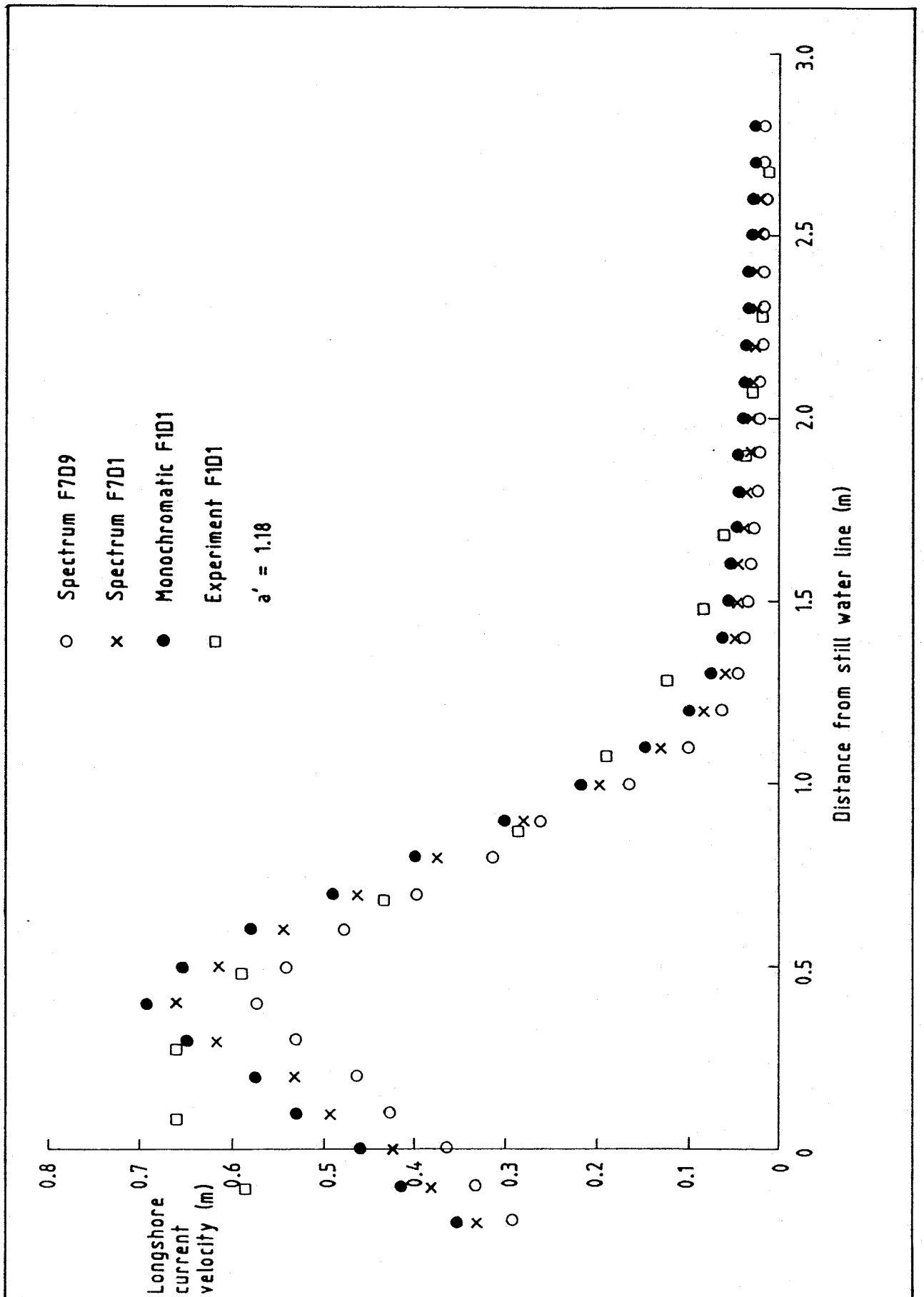
Fig 6   Laboratory tests – Top-Hat spectrum – longshore current velocities
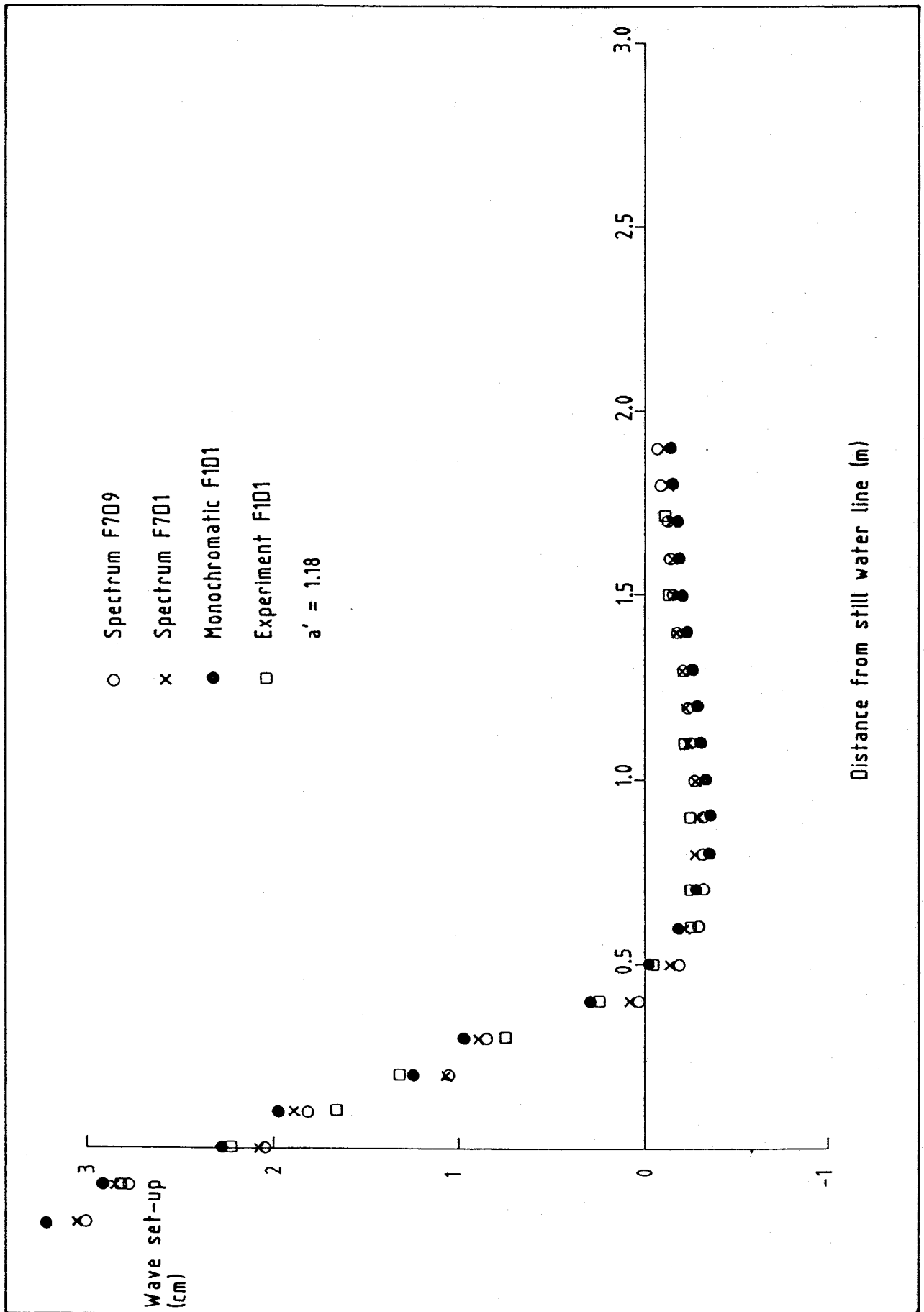
Fig 7   Laboratory tests – Top-Hat spectrum – wave set-up
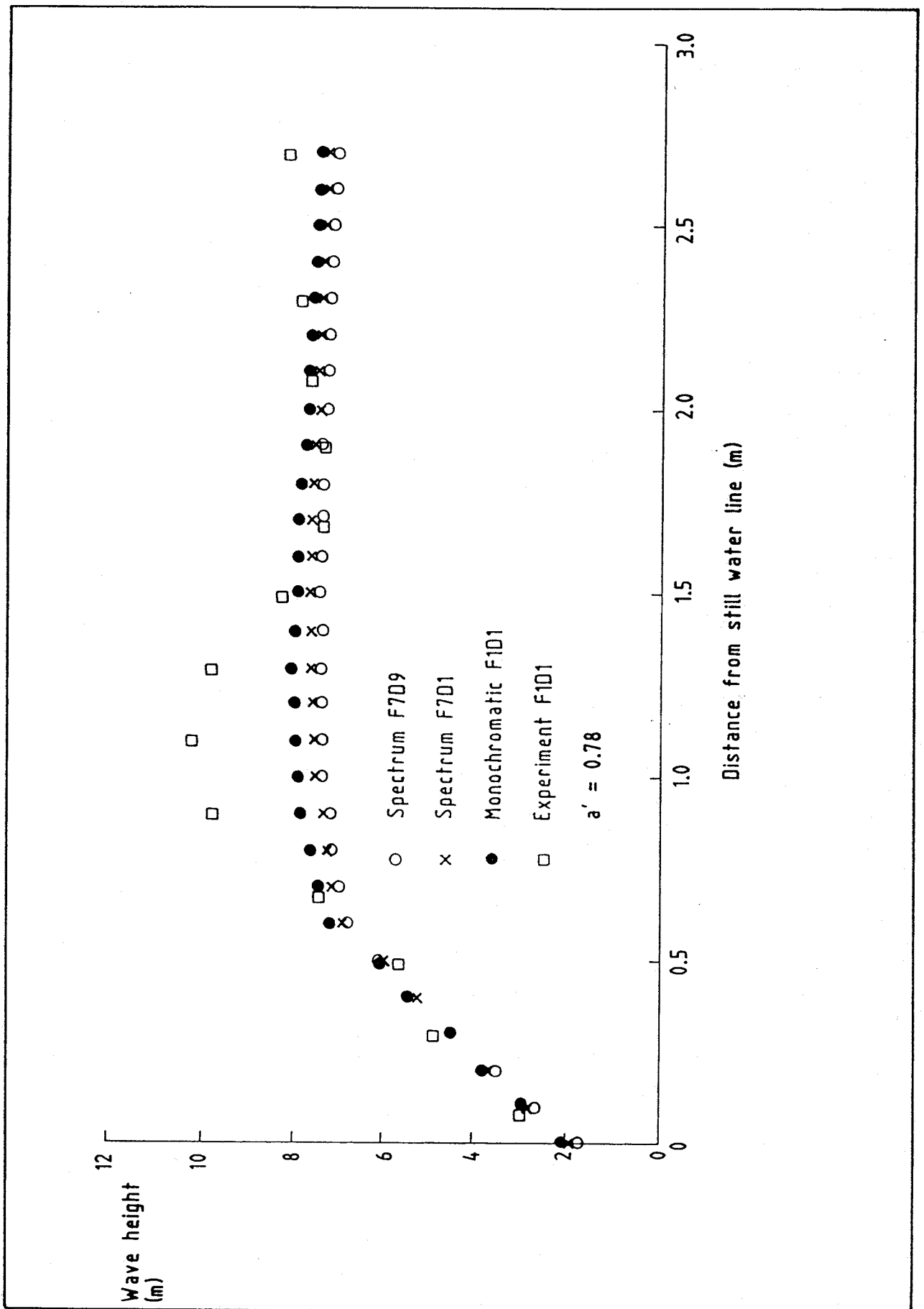
Fig 8   Laboratory tests – Top-Hat spectrum – wave heights (RMS values for spectra)
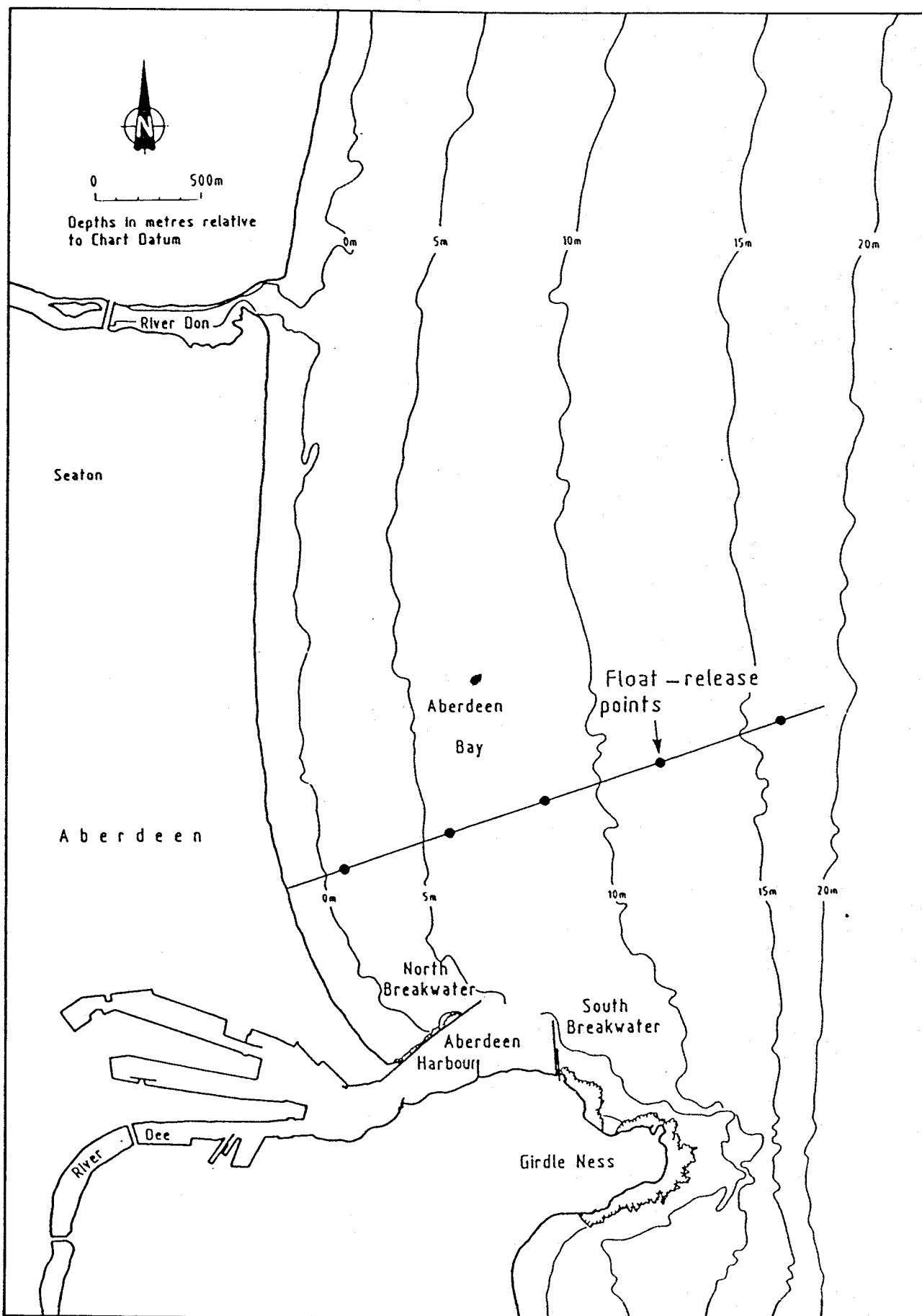
Fig 9   Location of profile line for field tests
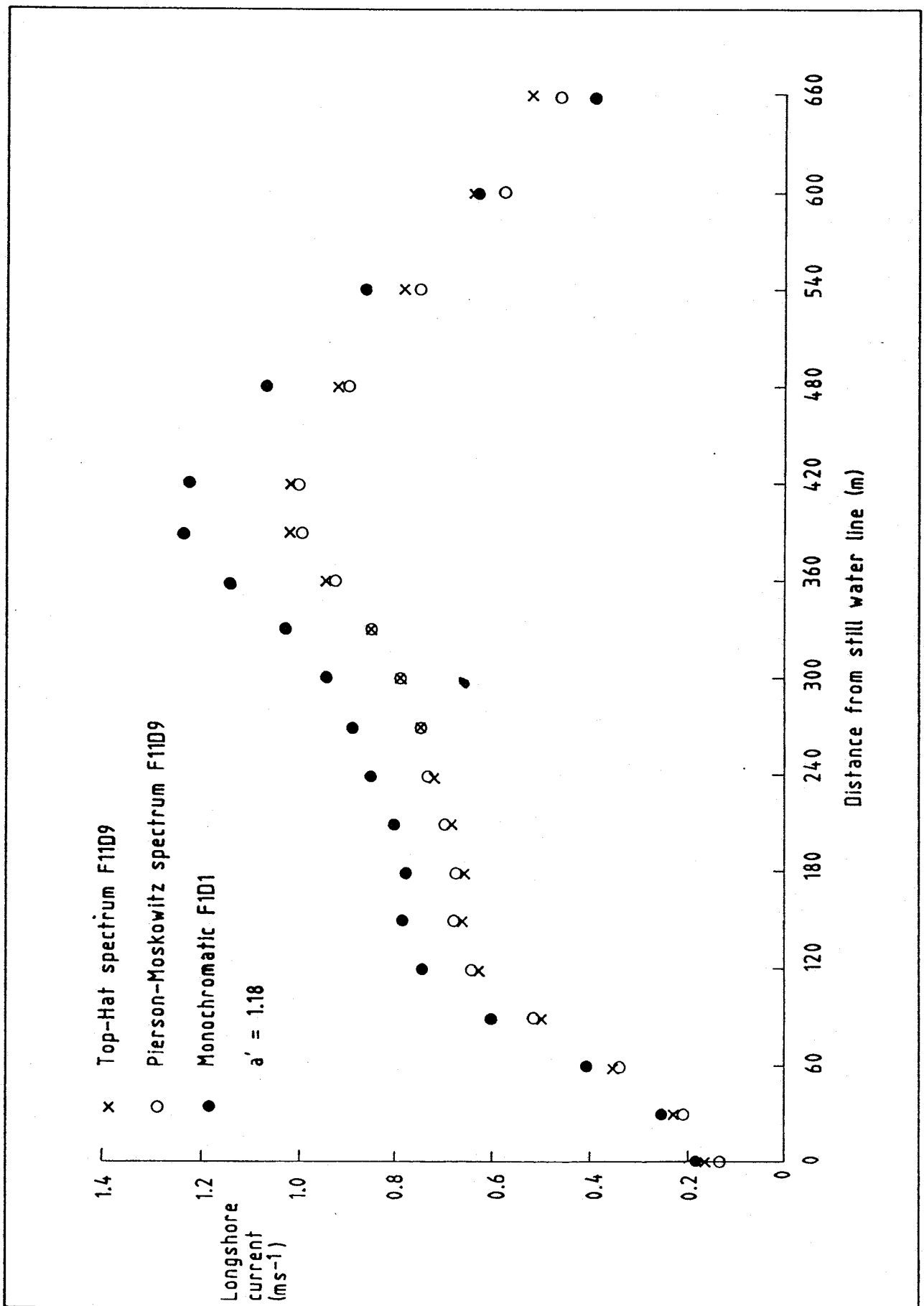
Fig 10   Field tests – longshore current velocities
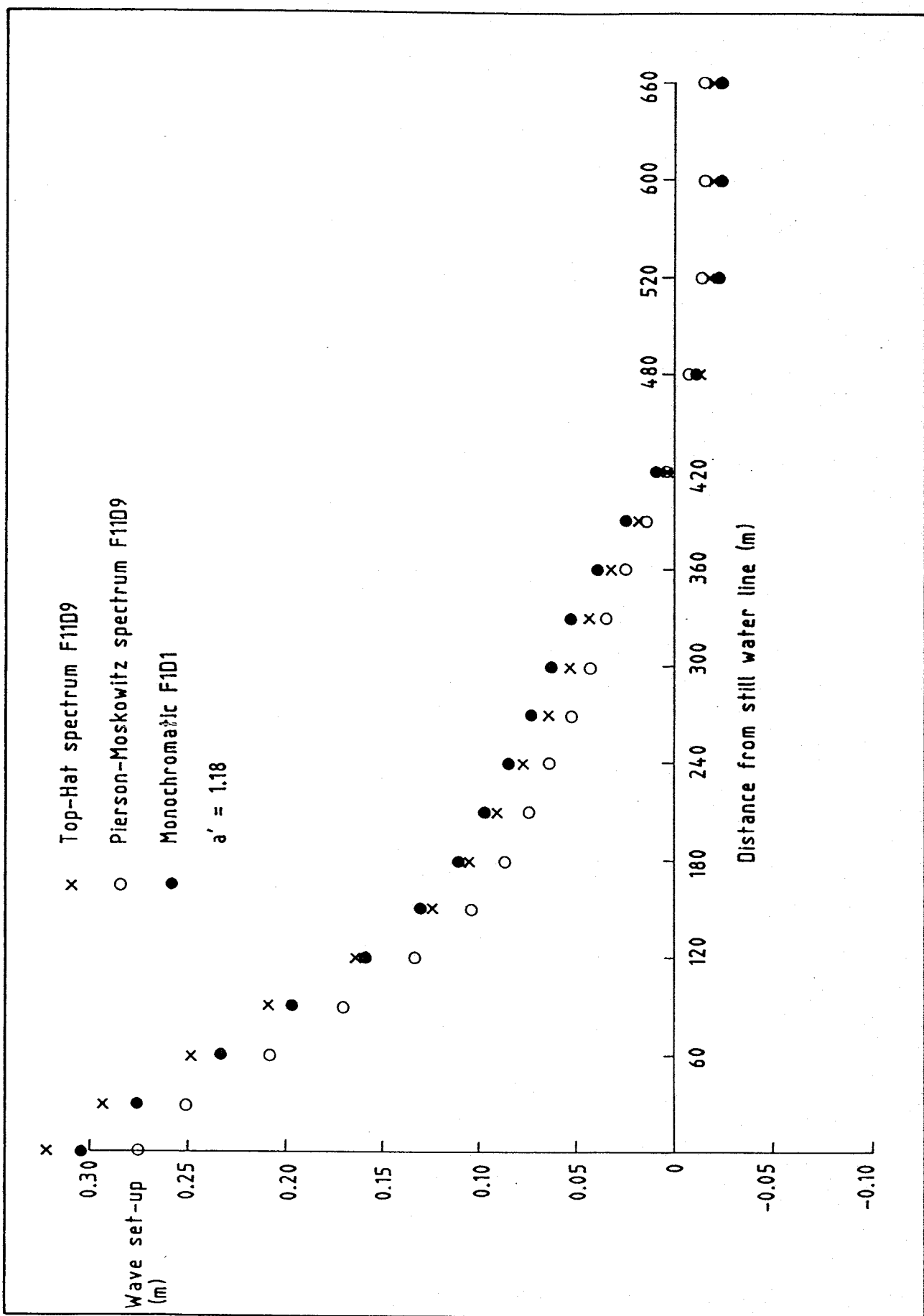
Fig 11   Field tests – wave set-up

Fig 12   Field tests – wave heights (RMS values for spectra)